Int. J. Electrochem. Sci., 2 (**2007**) 883 - 896

International Journal of ELECTROCHEMICAL SCIENCE
www.electrochemsci.org

Effect of Microestructure on the CO_2 Corrosion Inhibition by Carboxyamidoimidazolines on a Pipeline Steel

J. G. Gonzalez-Rodriguez[1], T. Zeferino-Rodriguez[1], D.M. Ortega,[1] S. Serna[1], B. Campillo[2], M.Casales[2], E. Valenzuela[3] and J. A. Juárez-Islas[4]*

[1] UAEM-CIICAp, Av. Universidad 1001, Col. Chamilpa, 62210-Cuernavaca, Mor. Mexico
[2] Universidad Nacional Autonoma de México, Instituto de Ciencias Físicas, Av. Universidad S/N, Col. Chamilpa, 62210-Cuernavaca, Mor., México
[3] Universidad Politécnica de Chiapas, Cuerpo Academico de Energía y Sustentabilidad Eduardo J.Selvas S/N ,Col. Magisterial,Tuxtla Gutiérrez Chiapas
[4] Universidad Nacional Autonoma de México, Instituto de Inv. En Materiales, Circuito Interior, México, D.F., México
[*]E-mail: ggonzalez@buzon.uaem.mx

Received: 28 August 2007 / *Accepted:* 7 September 2007 / *Online published:* 5 October 2007

The corrosion inhibition of carboxy-amidoimidazoline was evaluated by using potenthiodynamic polarization curves, linear polarization resistance and electrochemical impedance spectroscopy techniques. Solution included deaerated 3% NaCl saturated with CO_2 at 50°C. Material tested was a pipeline steel with three different microestructures obtained by thermo mechanical processing, namely martensitic, ferritic with bainite island and a ferritic. Results showed that in uninhibited solution, the martensitic steel exhibited the highest corrosion rate but in inhibited solutions, the martensitic steel had the lowest corrosion rate and the ferritic one had the highest dissolution rate. Results showed that a high density of fine carbides homogenously distributed improved the dissolution rate.

Keywords: CO_2 corrosion, pipeline steel, imidazoline, microstructure

1. INTRODUCTION

Corrosion is one of the most serious problems in the oil and gas production and transportation industry. Oilfield corrosion manifests itself in several forms, among which CO_2 corrosion (sweet corrosion) and hydrogen sulfide (H_2S) corrosion (sour corrosion) in the produced fluids and corrosion by oxygen dissolved in water injection are by far the most prevalent forms of attack found in oil and gas production [1].

The use of inhibitors is currently used to protect against corrosion in all petrochemical facilities in the world, because it is cost-effective and flexible. Nitrogen-based organic inhibitors, such as imidazolines or their salts have been successfully used in these applications even without an understanding of the inhibition mechanism [2-4]. The corrosion inhibition of organic compounds is related to their adsorption properties. Adsorption depends on the nature and the state of the metal surface, on the type of corrosive environment and on the chemical structure of the inhibitor [5]. Studies report that the adsorption of the organic inhibitors mainly depends on some physico-chemical properties of the molecule, related to its functional groups, to the possible steric effects and electronic density of donor atoms; adsorption is suppose also to depend on the possible interaction of the π-orbitals of the inhibitor with the d-orbitals of the surface atoms, which induce greater adsorption of the inhibitor molecules onto the surface of metal, leading to the formation of a corrosion protection film [6].

The interaction between the molecular structure of the inhibitors and the influence of steel microstructure in their performance is rarely studied, even though its great importance in field applications. According to Rosenfield et al. [7], inhibitors incorporate to the corrosion product layer and form a protective barrier between the base material and the corrosive media. French et al [8] presented SEM results showing that the structure of the corrosion products layer is modified by the inhibitors. They suggested that the structure of the inhibitor must be appropriate one to interact with the corrosin products and that they can be effective on iron carbonates or sulfides, but not effective on oxides. Oblonsky et al [9] studied the adsorption of octadecyldimethylbenzylammonium chloride (ODBCA) to carbon steel with two different microestructures. They found that ODBCA physisorbs strongly to the ferritic-perlitic microstructure and weakly to the martensitic microstructure. They attributed the difference to the persistency of the passive films on the microstructures, with the more stable film on the martensitic steel preventing optimal adsorption of the inhibitor.

The purpose of this paper is to evaluate the behaviour of a carboxy imidazolines as corrosion inhibitors in the CO_2 corrosion of a pipeline steel under three different microstructures using electrochemical technique in an environment containing NaCl, CO_2 to simulate environments found in the transport of crude oil.

2. EXPERIMENTAL PART

2.1. Test material

Material tested was a pipeline with a chemical composition as given in table 1. Samples of 0.030 x 0.010 x 0.30 m were heated at 1250 ºC, at a heating rate of 0.4 ºC/s, soaked for 90 minutes and immediately hot rolled. The rough rolling of the slab was performed from 1250 °C to 1098 ºC in 5 passes, reaching 42.3 % of total deformation and an average strain rate of 2.48 s^{-1}. Then, the rough rolling was followed by a cooling period until an experimental initial temperature for the final rolling procedure of 1051 ºC was reached, ending at 867 ºC, achieving a total deformation of 37 % in 5 passes with an average strain rate of 2.98 s^{-1}. Immediately after the last final rolling pass, the plates were cooled in forced nitrogen gas, water sprayed or water quenched. The first and second cooling

procedures were performed from 867ºC to 650ºC and then the plates were let to cool in air to room temperature. Before testing, the electrode was polished to 600 grit SIC emery paper and then cleaned with alcohol, acetone and distilled water.

Table 1. Chemical composition of studied steel

C	Si	Mn	P	S	Cr	Ni	Ti	V	Cu	Nb	Mo	Al
0.044	0.271	1.69	0.009	0.001	0.010	0.240	0.014	0.001	0.217	0.055	0.25	0.0310

2.2. Test solution

Inhibitor used in this work was a commercial carboxy-amidoimidazoline with a general structure as shown on Fig. 1. Inhibitor was dissolved in pure 2-propanol. The concentration of the inhibitor used in this work was 25 ppm and the temperature kept at 50°C. Before applying the inhibitor, a solution containing 3% NaCl was prepared. The testing solution consisted of 3% NaCl solution, heated, deaerated with nitrogen gas, CO_2 saturated for two hours, and then the inhibitor added. Continuous stirring was used and CO_2 bubbled during the tests.

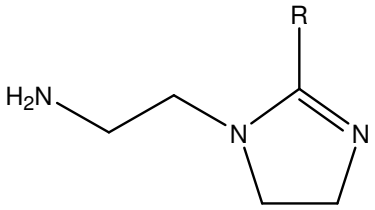

Figure 1. Schematic diagram showing chemical molecular structure of the used inhibitor.

2.3. Electrochemical measurements

Electrochemical techniques employed included poltenthiodynamic polarization curves, linear polarization resistance, LPR, and electrochemical impedance spectroscopy, EIS, measurements. Polarization curves were recorded at a constant sweep rate of 1 mV/s and the scanning range was from -300 to +300 mV respect to the open circuit potential, E_{corr}. Measurements were obtained by using a conventional three electrodes glass cell with two graphite electrodes symmetrically distributed and a saturated calomel electrode (SCE) as reference with a Lugging capillary bridge. Inhibition efficiencies (*E(%)*) were determined from the corrosion current densities calculated by the Tafel extrapolation method according to the following equation

$$E(\%) = \frac{i_i - i_b}{i_i} \text{X } 100 \qquad (1)$$

where i_b is the corrosion rate without inhibitor and i_i the corrosion rate in the solution with inhibitor.

LPR measurements were carried out by polarizing the specimen from +10 to –10 mV respect to E_{corr}, at a scanning rate of 1 mV/s. Inhibition efficiencies [*E(%)]* were determined according to the following equation

$$E(\%) = \frac{R_{p,i} - R_{p,b}}{R_{p,i}} \text{X } 100 \qquad (2)$$

where $R_{p,b}$ is the linear polarization resistance without inhibitor and $R_{p,i}$ is the linear polarization resistance with inhibitor. Electrochemical impedance spectroscopy tests were carried out at E_{corr} by using a signal with an amplitude of 10 mV and a frequency interval of 0.1-100KHz. An ACM potentiostat controlled by a desk top computer was used for the LPR tests and polarization curves, whereas for the EIS measurements, a model PC4 300 Gamry potentiostat was used.

3. RESULTS AND DISCUSSION

Microestructures resulting from the different thermomechanical heat treatments consisted basically, for material 2F, of a martensitic microstructure with fine fine carbides, nanometer size, homogenously distributed. Carbides were found both between martensithe laths and inside some ferrite grains. Steel 1T had a ferritic micriestructure with some bainitic areas and some carbides. These carbides were bigger than the ones found on steel 2F and were located on the grain boundaries Finally, steel 2A had acicular ferrite plus some bainitic areas; this time carbides were much finer than the ones found in steels 2A but similar to the ones found on steel 2F but they were found mainly inside the grain boundaries, whereas some of them were found inside the ferrite grains.

Table 2. Electrochemical parameters for the different steels exposed to a CO_2 saturated 3% NaCl solution with without the addition of inhibitor

Sample	**E_{corr} (mV)**	**i_{corr} (mA cm^{-2})**	**b_a(mV/decade)**
1T	-675	$2X10^{0}$	63
2A	-715	$5X10^{-1}$	53
2F	-715	$5X10^{-1}$	57

Table 3. Electrochemical parameters for the different steels exposed to a CO_2 saturated 3% NaCl solution with the addition of 25 ppm of inhibitor

Sample	**E_{corr} (mV)**	**i_{corr} (mA cm^{-2})**	**b_a(mV/decade)**	***E(%)***
2A	-625	$^{1}1.5X10^{-1}$	17	85
2F	-615	$3X10^{-2}$	23	95
1T	-615	$1X10^{-}$	33	94

Fig. 2 shows the polarization curves for all steel in the CO_2saturated 3% NaCl without and with the addition of 20 ppm of inhibitor. Electrochemical parameters for these curves are given on tables 2 and 3 respectively. These curves show that the E_{corr} value shifted towards more noble values and the I_{corr} values were decreased for almost one order of magnitude with the inhibitor Practically all

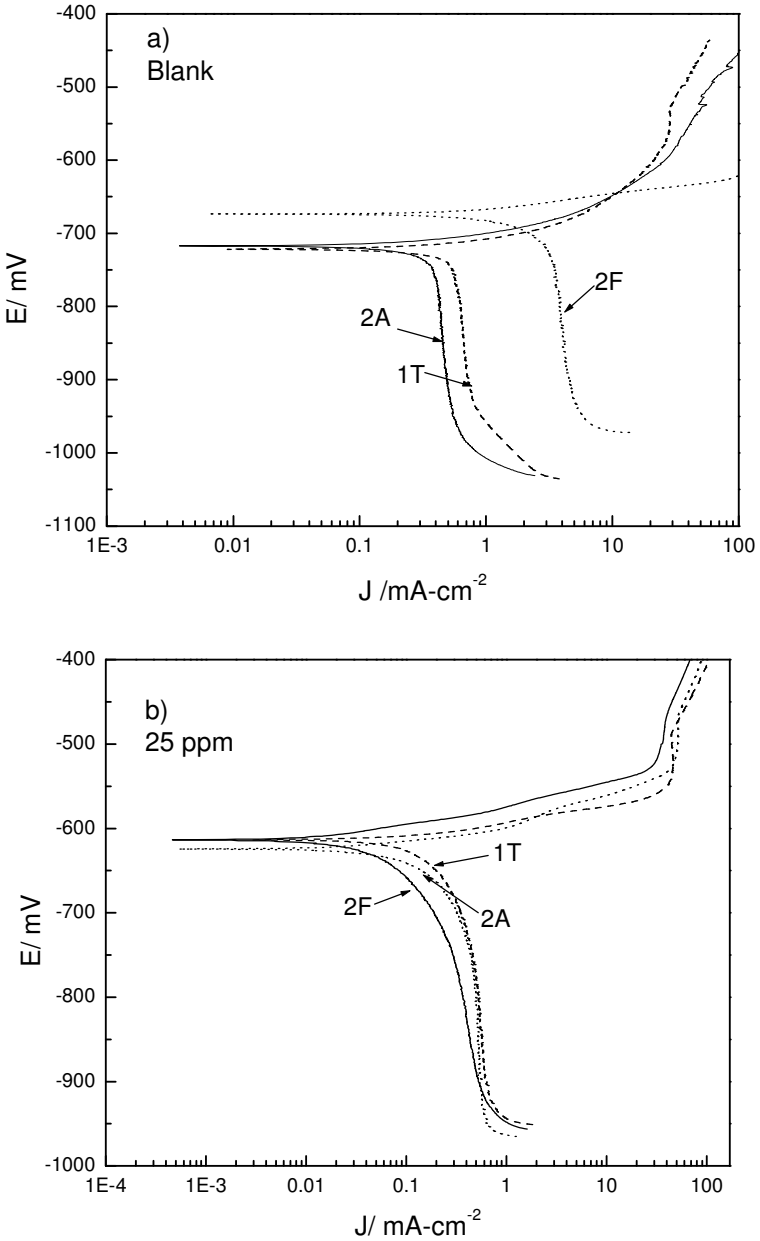

Figure 2. Polarization curves for steels 1T, 2A and 2F in a CO_2-saturated 3% NaCl solution a) without inhibitor and b) with 25 ppm inhibitor.

the anodic branch of the polarization curves were identical for the different steels, The linear Tafel region appeared only on the anodic branch, but on the cathodic branch only a diffusion limiting current density was observed, which indicated that the imidazoline could be absorbed in the metal

surface without applying any potential on the electrode. This cathodic limit current can be due to a decrease on the H^+ ions concentration near the metallic surface and to a slow hydratation of the CO_2.so the reported I_{corr} values on table 2 and 3 are approximated ones calculated by extrapolating the anodic Tafel slope to the free corrosion potential. In any case, difference between the corrosion current density values for the inhibited and the uninhibited solutions, one order of magnitude, justify the Tafel extrapolation. The highest efficiency was obtained for steel 2F, with 95%, practically the same as that for steel1T, with 94%, whereas the lowest one was for steel 2A, with 85%.

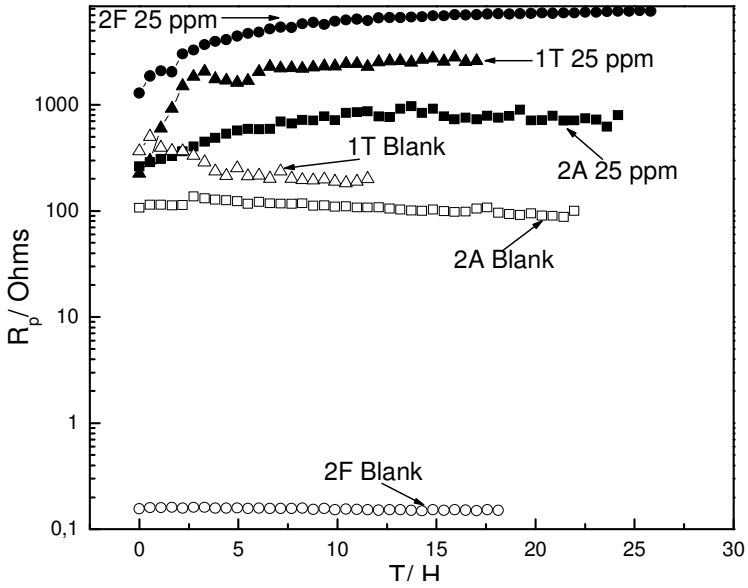

Figure 3. Change in the R_p values for steels 1T, 2A and 2F in a CO_2-saturated 3% NaCl solution without and with 25 ppm inhibitor.

These findings were confirmed by the LPR results, as shown on Fig. 3, where it can be seen that the lowest LPR value, and thus, the highest corrosion rate value, was obtained for the steel 2F in the solution without inhibitor, but at the same time, when the inhibitor was added, this same steel obtained the highest LPR value. This figure also shows that the LPR values in the uninhibited solution remained constant with time, whereas for the inhibited solution, these values increased with time until reaching a constant value, probably due to the formation and stabilization of a film. Calculated efficiencies by using Eq. 2 at 24 of immersion for steel 1T was 92.52%, 87.33 for steel 2A and 99.99% for steel 2F. Thus, it is obvious that the microstructure plays a key role in the effectiveness of a corrosion inhibitor.

The Nyquist data for the uninhibited 3% NaCl solution are given in Fig. 4 for the three steels. The impedance spectra exhibited in all cases a single (capacitive like) depressed semicircle. The semicircle diameter practically remained constant with time, indicating that the corrosion rate was not reduced with time, as evidenced by the LPR tests on Fig. 3. Bode diagrams in the phase angle versus log(frequency) format for the three steels was identical and it showed a single phase angle shift at 100 Hz, with this peak shifting towards lower frequencies as time elapses, as shown on Fig. 5. There is no evidence of the formation of a protective film because there is only one capacitive loop in the EIS

Nyquist plots [11]. One would expect to see a new phase angle shift at higher frequency range and a continuous increase in the phase angle shift with time during film formation.

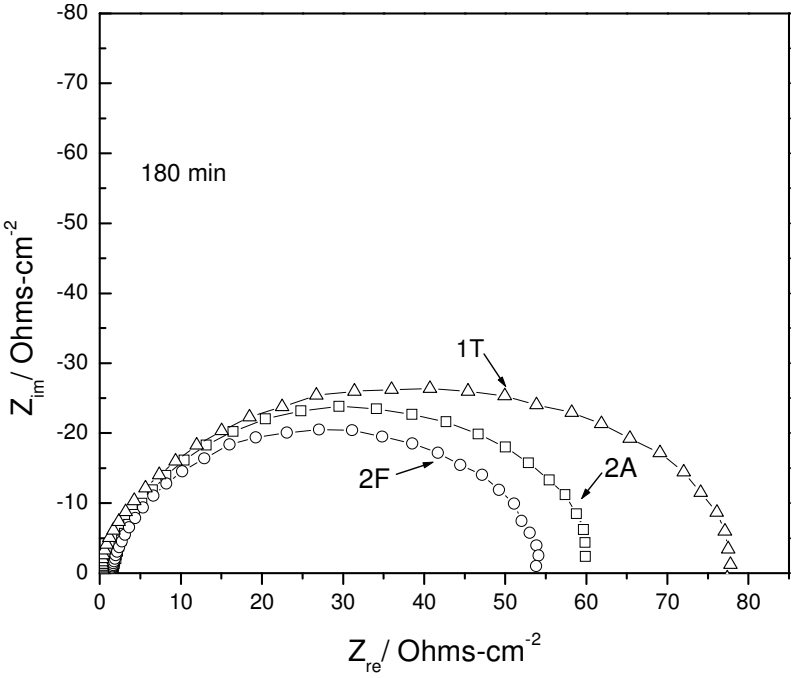

Figyre 4. Nyquist diagrams for steels 1T, 2A and 2F in a CO_2-saturated 3% NaCl uninhibited solution.

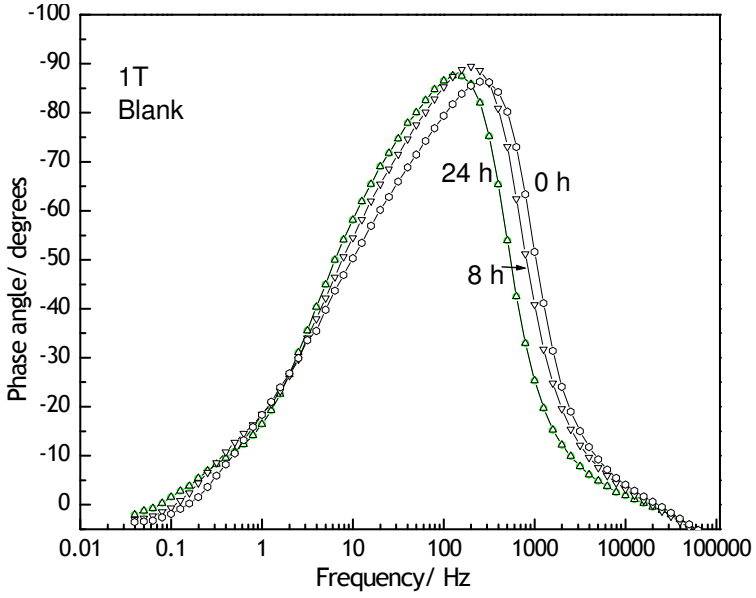

Figire. 5. Bode diagrams for steels 1T, in a solution without inhibitor.

Nyquist results for inhibited solution for steel 2A and 1T were very similar, and the corresponding one for steel 2A is shown on Fig. 6. Spectra formed depressed semicircles with a diameter value increasing as time elapses and the center under the real axis. The magnitude of the

impedance with is up to 4 orders of magnitude higher than the impedance obtained for the uninhibited solution. This is expected since the inhibitor used was oil soluble and thus, the inhibitor would be transported to the surface when the oily part was present.

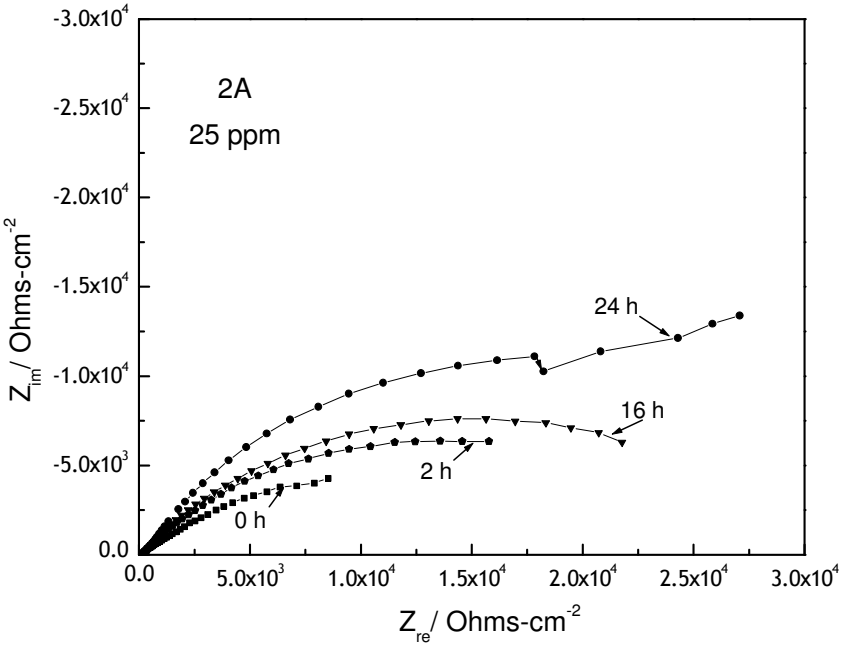

Figure 6. Nyquist diagrams for steels 2A in a CO_2-saturated 3% NaCl solution with 25 ppm Inhibitor.

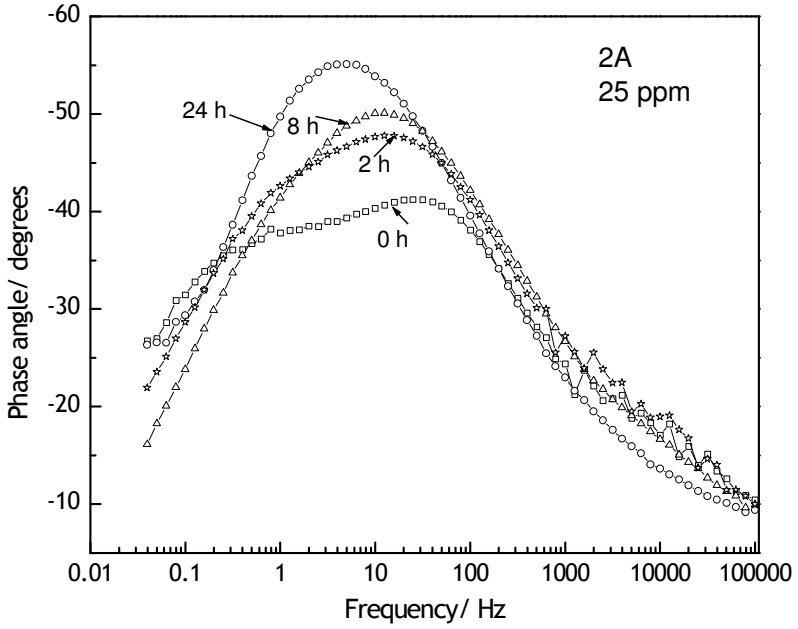

Figure 7. Bode diagrams for steel 2A in a CO_2-saturated 3% NaCl solution with 25 ppm Inhibitor

Bode diagrams for steel 2A is shown on Figs. 7 . It can be seen that steel 2A shows two peaks at 1 and 100 Hz, indicative of a protective film. As time elapses, the peak at 1 Hz disappears after two hors and the one at 100 Hz shifts towards lower frequencies, indicating that the protective film

disappear. Steel 1T had a similar behavior, but the time that the protective film disappears is longer than that for steel 2A, indicating that the protective film is more stable with this steel.

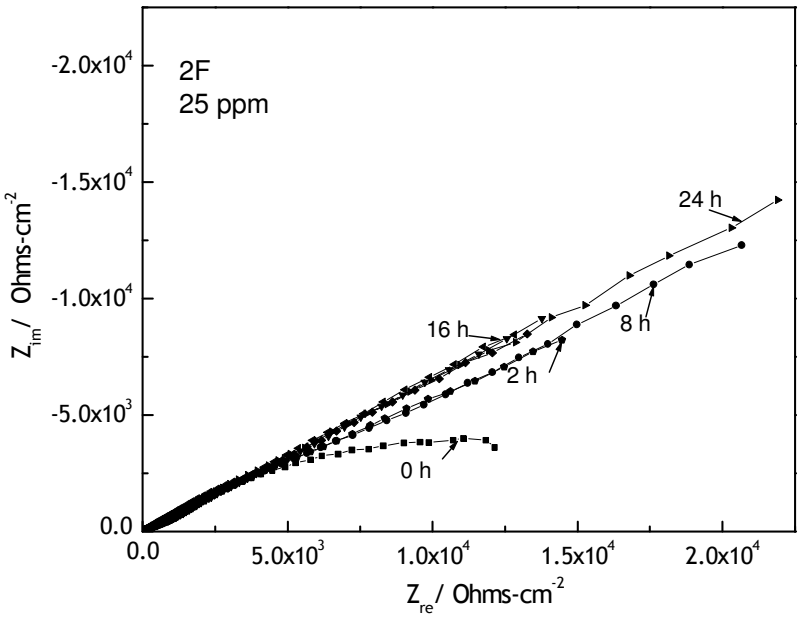

Figure. 8. Nyquist diagrams for steels 2F in a CO_2-saturated 3% NaCl solution with 25 ppm Inhibitor

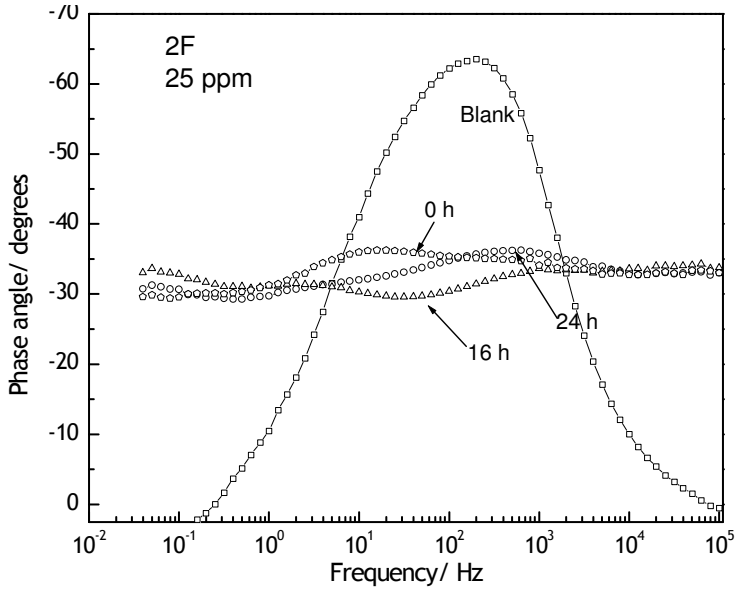

Figure 9. Bode diagrams for steels 2F in a CO_2-saturated 3% NaCl solution with 25 ppm Inhibitor

Nyquist diagram for steel 2F is shown on Fig. 8 and its corresponding Bode diagram is shown on Fig. 9. Nyquist diagram show a depressed semicircle only at the beginning of the test, but after 2 hours of testing, only a straight line is obtained. These plots show a charge transfer mechanism is not any longer the dominant mechanism and it has changed to a diffusion controlled reaction, which may

be due to the transport of ions in solution which slowly replaces charge transfer. Bode diagram shown on Fig. 9 shows a single phase angle shift around 100 Hz for the blank solution, but once the inhibitor is added, the phase plot shows a new phase angle shift at higher frequencies, which was more pronounced with increasing time. The existence of the two-phase angle shifts in the Bode diagram suggests that there are two main kinetic processes on the electrode surface. Being consistent with other authors [12,13] the high frequency loop can be ascribed to the inhibitor film because of its small time constant causes a phase shift in the higher frequency limit. According to these authors, the presence of long hydrocarbon chains in the structure of the imidazolines is responsible of their capacity of forming protective barriers against aggressive ions from the bulk solution.

Electrically equivalent circuits are generally used to model the electrochemical behavior and calculate the parameters of interest such as electrolyte resistance (R_s), charge transfer resistance (R_{ct}) and double layer capacitance (C_{dl})[14]. When a non-ideal frequency response is present, it is commonly accepted to employ distributed circuit elements in an equivalent circuit. The most widely used is constant phase element (CPE), which has a non-integer power dependence on the frequency. The impedance of a CPE is described by the expression:

$$Z_{CPE} = Y^{-1} (iw)^{-n} \quad (3)$$

where Y is a proportional factor, i is $\sqrt{-1}$, w is $2\pi f$, f the frequency and n has the meaning of a phase shift(14). Often a CPE is used in a model in place of a capacitor to compensate for non-homogeneity in the system to take into account irregularities of the surface such as roughness or because properties such as double layer capacitance, charge transfer rate, etc…are non uniformly distributed. For an ideal capacitor Y is 1/C and n = 1, whereas for a non ideal capacitor $n < 1$.

To describe the behaviour of impedance spectra which are under a coupled mechanism of charge transfer and diffusion of reactants, a diffusional impedance arises called Warburg impedance. The diffusional resistance, R_d is the low-frequency limit of the real part of the impedance, Z_{re}, and is given by :

$$R_d = \frac{\sigma (2\delta)^{1/2}}{D^{1/2}} \quad (4)$$

where σ is the Warburg coefficient and is given by

$$\sigma = \beta/[nFC_s(2D)^{1/2}] \quad (5)$$

with δ as the thickness of the diffusion layer, D is the diffusion coefficient of the species involved, β the cathodic Tafel slope and C_s the surface concentration of reactants.

The impedance spectra obtained in this work can be modeled as electric equivalent circuits given in Fig. 10. The data obtained for uninhibited solutions can be modeled by circuit shown on Fig.

10 a. This is a simple circuit for the corrosion system under charge transfer control, where no mass transport were detected. The fitting parameters for steel 2A in this solution appear as solid lines on Figs. 5 and 6 showing a good fit.

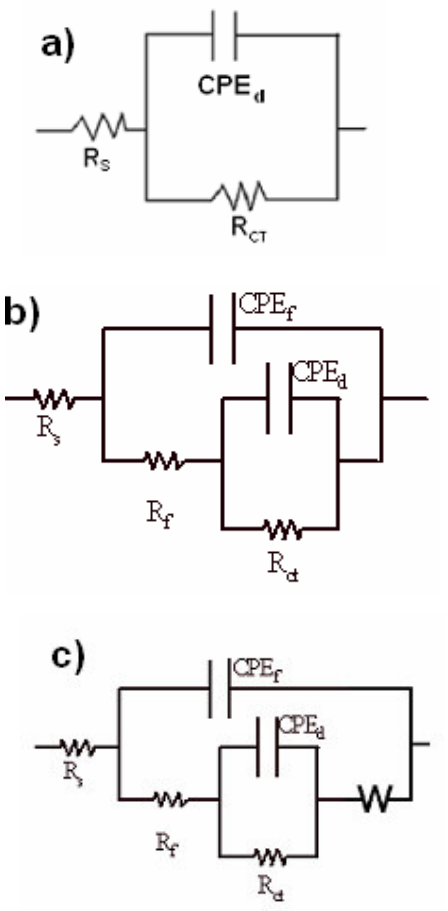

Figure 10. Equivalent circuits used to model EIS data a) uninhibited solutions, b)inhibited solutions for steels 1T and 2A and c) inhibited solutions for steels 2F.

For steels 1T and 2A under inhibited solutions, the EIS data were modeled by using electric circuit shown in Fig. 10 a and b. On Fig. 10 b R_f and CPE_F represent the resistance and capacitance of a formed inhibitor film on the surface. As exhibited by Bode diagrams shown on Figs. 6 and 7, for steel 2A there is evidence of a formed inhibitor film during the first two hours, whereas for steel 1T this film lasts at least 8 hours. For this time when a inhibitor film is formed, circuit shown on Fig. 10 b gave the best fit. However, after some time this film is destroyed, as evidenced by Figs. 6 and 7, and electric circuit to model EIS data is the one shown on Fig. 10 a.

On the other hand, for steel 2F, circuit shown on Fig. 10 c was used to simulate the EIS spectra. On this case, the existence of a Warburg-type impedance arises, indicating that the corrosion process is under diffusion control. Figs. 11 and 12 show the trend of R_f and R_{ct} with time respectively for the tree steels. It can be seen that both parameters follow some how the same trend, for steel 1T both parameters tend to decrease with time until reaching a steady state value, whereas for steels 2A and 2F

both the inhibitor film resistance, R_f, and the charge transfer resistance, R_{ct} tend to increase with time. Until they reach a steady state value. The highest values for both parameters were for steel 2F, the one with a martensitic microstructure, whereas the lowest values were for steel 1T, the one with a ferritic micorestructure mainly.

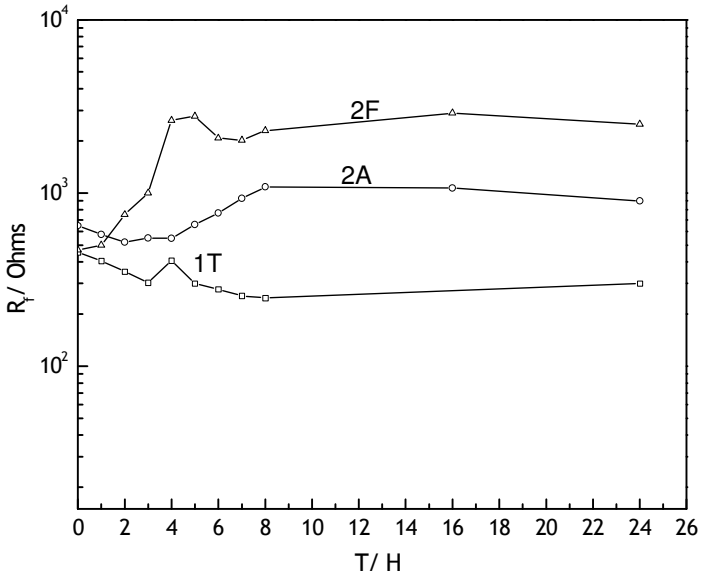

Figure 11. Change in the film resistance, R_f, with time for steels 1T, 2A and 2F in a CO_2-saturated 3% NaCl solution with 25 ppm inhibitor

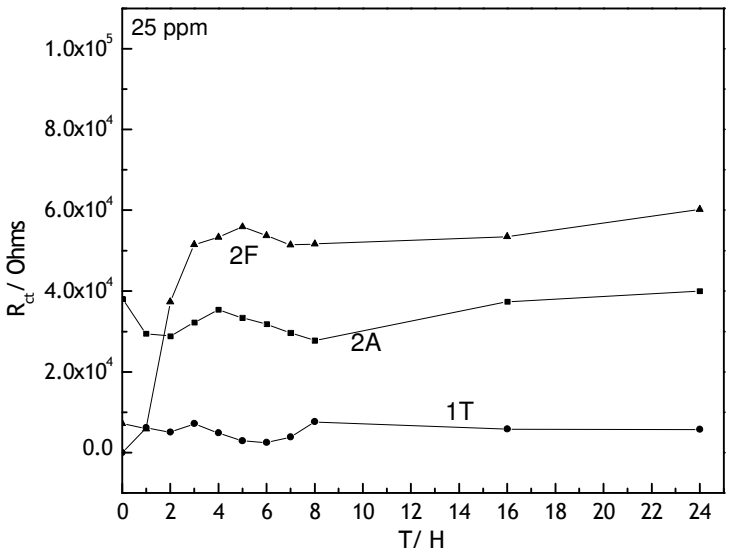

Figure 12. Change in the charge transfer resistance, R_{ct}, with time for steels 1T, 2A and 2F in a CO_2-saturated 3% NaCl solution with 25 ppm

CO_2 corrosion of carbon and low alloy steels is strongly dependent on the surface films formed during the corrosion processes. The protectiveness, rate of formation/precipitation, and the stability of

the film controls the corrosion rate and its nature. The main film formed during CO_2 corrosion of iron and low alloy steels is iron carbonate, $FeCO_3$, which is affected by iron and carbonate concentrations and temperature dependent. All authors agree that increasing the temperature would improve the protectiveness of the $FeCO_3$ scales as well as its adherence and hardness[15]. The lowest temperature necessary to obtain $FeCO_3$ films that would reduce the corrosion rate is 50°C. Inhibitor film will be formed and anchored on top of this $FeCO_3$ film, which, in turn, will depend, among other factors, upon the microstructure of the steel[16, 17]. The scale grown on normalized steels with a ferritic-perlitic microstructure was more adherent, having larger crystals more densely packed and thicker than those formed on quenched and tempered steels[18]. The ferritic-perlitic steels have a carbide structure which gives a good framework for the buildup of protective carbonate films[19]. Quenched and tempered steels and ferritic steels with low carbon content have a finely distributed carbide structure that does not give an integrated framework to anchor and enhance the formation of protective carbonate films[19, 20]. Experiments with plain carbon steels after different heat treatments showed that both corrosion rate and the ability to form protective iron carbonate films decrease with increasing tempering temperature, indicating that the steel microstructure plays an important role for the formation of protective corrosion films. However, the opposite has been reported also[18,21].

The anchoring effect of the microstructure, and more than the microstructure, carbide size and distribution, is believed to be the main factor influencing the adhesion of the iron carbonate film on the surface that has been reported by many authors. The stability of the formed inhibitor film will depend, thus upon the adherence of the corrosion product formed. For example, Dugstad[20], working with a similar low alloy carbon steel with different heat treatments, found that the adherence of the corrosion film is related to the anchoring effect of carbides. When the corrosion rate was low, the corrosion product was composed mainly by $FeCO_3$, but when the corrosion rate was higher, the corrosion product was formed by $FeCO_3$ plus cementite, Fe_3C. The quenched steel containing no carbides and the non-heat treated steel with the largest carbide particles had the lowest corrosion rates. In our case, steels 2F and 1T

It is uncertain why the protective corrosion rate increased when there exist large carbide particles, but one explanation is that when the particle size is small, there is a higher number of particles and thus, a larger number of anchoring sites for the protective film. It has also been suggested that defects in the metal structure can facilitate the anchoring of the film, but this has not been confirmed. Microstructures showed that the highest number of carbides and more homogenously distributed, and thus, the number of sites for film anchoring is observed for steel 2F, the steel 2A had many fine carbides, but along grain boundaries, and not inside the grains, thus a lower number of sites for film anchoring, and this steel presented the highest corrosion rate. Thus, this difference in carbide size and distribution could explain the corrosion behavior of the three steels: that steel with a homogenous distribution of high density of fine carbides presented the lowest corrosion rate, and conversely, that steel with a less amount of carbides, bigger in size, or distributed in a heterogeneous way, will present a higher corrosion rate

4. CONCLUSIONS

The corrosion behavior of a steel with three different microestructures, martensitic, ferritic and bainitic and a ferritic one has been evaluated in CO_2-saturated 3% NaCl solution at 50°C. Results showed that in uninhibited solution, the martensitic steel exhibited the highest corrosion rate whereas the others two had similar corrosion rate. However, in inhibited solutions, the martensitic steel had the lowest corrosion rate and the ferritic one had the highest dissolution rate. The martensitic steel had a high density of fine carbides, homogenously distributed, whereas the ferritic one had fine carbides mainly along the grain boundaries and the ferritic and bainitic steel had carbides of bigger size along the grain boundaries.

References

1. M.B. Kermani and A. Morshed, *Corrosion* 59 (2003) 659.
2. V. Jovancicevic, S. Ramachandran and P. Prince, *Corrosion* 55 (1999) 449.
3. Ramachandran S and Jovancicevic V., *Corrosion* 55 (1999) 259.
4. Z. Xueyuan, *Corrosion Science* 43 (2001) 1417.
5. F. Bentiss, M. Lagrenee, M. Traisnel, J.C. Hornez, *Corros. Sci*. 41, (1999) 789.
6. F. Bentiss, M. Traisnel, M. Lagrenee*, J. Appl. Electrochem*. 31, (2001) 449.
7. I.L. Rosenfield, D.B. Bogomolov, A.E. Gorodetskii, L.P. Kazanszkii, L.V. Frolova, L.I. Shamova, Z. *Metallakd* 18 (1982) 163.
8. E.C. French, R.L. Martin, J.A. Dougherty, MP 28 (1989) 46.
9. L.J. Oblonsky, G.R. Chesnut, T.M. Devine, *Corrosion* 51 (1995) 891.
10. F.D. de Moraes, J.R. Shadley, J. Chen, E. Rybicki, in Proceedings of the NACE Corrosion/2000, NACE 2000, Orlando FL, 2000, Paper No. 30.
11. G.W. Walter, *Corros. Sci*., 26 (1989) 681.
12. D. Wang, S. Li, M. Ying, M. Wang, Z. Xiao, Z. Chen, *Corros. Sci*, 41 (1999); 1911.
13. F. Mansfield, *Electrochim. Acta* 35 (1990) 1533
14. J.R. Macdonald*, J Electroanal. Chem*. 223 (1987) 25.
15. K. Videm, A : Dugstad, *Mater. Perform*. 4 (1989) 46.
16. M.B. Kermani, L.M. Smith eds. Predicting CO_2 corrosion in the oil and gas industry. European Federation of Corrosion Publication No. 13 (London, U.K., Institute of Materials, 1994).
17. M.B. Kermani, L.M. Smith eds. Predicting CO_2 corrosion in the oil and gas industry-Design Considerations, European Federation of Corrosion Publication No. 23 (London, U.K., Institute of Materials, 1997).
18. C.A . Palacios, J.R. Shadley, *Corrosion* 47 (1991) 356.
19. D.E. Cross, « Mesa-Type CO_2 Corrosion and its Control »,CORROSIION/93, Paper 118, (Houston, TX, NACE, 1993).
20. A. Dugstad, H. Hemmer, M.Sefesten, « Effect of Steel Microestructure upon Corroson Rate and Protective Iron Carbonate Film Formation » CORROSIION/2000, Paper 23, (Houston, TX, NACE, 2000).
21. G.B. Chitwood, W.R. Coyle, R.L.Hilts, « A Case-Hystory Analysis of Using Plain Carbon and Low Alloy Steels for Completion Equipment in CO_2 Service » CORROSIION/94, Paper 90, (Houston, TX, NACE, 1994).